GA–A22451

# SCIENTIFIC BASIS AND ENGINEERING DESIGN TO ACCOMMODATE DISRUPTION AND HALO CURRENT LOADS FOR THE DIII–D TOKAMAK

by
P.M. ANDERSON, A.S. BOZEK, M.A. HOLLERBACH,
D.A. HUMPHREYS, J.L. LUXON, E.E. REIS, and M.J. SCHAFFER

OCTOBER 1996

GA–A22451

# SCIENTIFIC BASIS AND ENGINEERING DESIGN TO ACCOMMODATE DISRUPTION AND HALO CURRENT LOADS FOR THE DIII–D TOKAMAK

by
P.M. ANDERSON, A.S. BOZEK, M.A. HOLLERBACH,
D.A. HUMPHREYS, J.L. LUXON, E.E. REIS, and M.J. SCHAFFER

This is a preprint of a paper to be presented at the 19th Symposium on Fusion Technology September 16–20, 1996, Lisbon, Portugal and to be published in the *proceedings*.

Work supported by
the U.S. Department of Energy
under Contract No. DE-AC03-89ER51114

GA PROJECT 3466
OCTOBER 1996

# Scientific Basis and Engineering Design to Accommodate Disruption and Halo Current Loads for the DIII–D Tokamak*

P.M. Anderson, A.S. Bozek, M.A. Hollerbach, D.A. Humphreys, J.L. Luxon, E.E. Reis, M.J. Schaffer

General Atomics, P.O. Box 85608, San Diego, California 92186-5608, USA

Plasma disruptions and halo current events apply sudden impulsive forces to the interior structures and vacuum vessel walls of tokamaks. These forces arise when induced toroidal currents and attached poloidal halo currents in plasma facing components interact with the poloidal and toroidal magnetic fields respectively. Increasing understanding of plasma disruptions and halo current events has been developed from experiments on DIII–D and other machines. Although the understanding has improved, these events must be planned for in system design because there is no assurance that these events can be eliminated in the operation of tokamaks. Increased understanding has allowed an improved focus of engineering designs.

## 1. DISRUPTION FORCES

Disruptions drive large electric currents in the vessel and associated components by two identified mechanisms: magnetic induction and contact with halo currents [1,2]. The J×B forces resulting when these currents cross the magnetic field can be very large, possibly damaging in-vessel components or the vessel itself. The global force is reacted magnetically to the external magnetic coils and their support structure. Disruptions also induce electric fields that can break down electrical insulation and allow current to flow in unplanned places. The present DIII–D design philosophy is to avoid all but low voltage standoff in plasma facing components and to ensure that induced currents follow a planned, safe path.

### 1.1. Induced Current Loads

The DIII–D vessel is all metal (Inconel 625) with no insulating breaks and relatively uniform conductance. Vessel current is magnetically induced in the toroidal direction by the time derivative of the poloidal magnetic flux and is limited by toroidal resistance. Toroidal vessel voltage is measured by 19 toroidal loops attached to the vessel outer surface. The loops also measure poloidal flux for plasma control and diagnostic purposes. Loop voltages at internal components are adjusted for the time derivative of the additional flux between the vessel and that component, calculated with the aid of 31 magnetic pickups on the inner vessel surface. The vessel and internal components are more resistive than inductive on the DIII–D disruption time scale (≥ 3 ms). Therefore, the toroidal current density is approximately $J_T = E_T/h$, where $E_T$ is the toroidal electric field and h the electrical resistivity. The corresponding load is $J_T \times B_P$, where $B_P$ is the poloidal magnetic field.

A review of disruption data confirms that the largest induced toroidal current loads are produced at the top and bottom of the vessel by vertical displacement events (VDE), in which the plasma moves vertically after loss of vertical control, shrinks in cross section as it is limited by top or bottom components, and finally disrupts at low *q*. The largest loads occur in the vicinity of the disruption (top or bottom), where magnetic coupling to the decaying plasma current loop is greatest. Because VDEs are rare in DIII–D, a semi-empirical scaling law was developed for $E_T$ by combining qualitative theory and available data [3]. This yields: $E_T \sim (B_T I_p)^{1/2}$, $B_P \sim (B_T I_p)^{1/2}$ at the moment of disruption, and force = $J_T \times B_P \sim B_T I_p$, where $I_p$ is the pre-disruption plasma current. This scaling is used to extrapolate from historic VDEs to the anticipated load from a VDE at maximum machine capability. Dynamic loads are calculated using actual VDE waveforms.

Eddy current loads can be important in components that are not toroidally continuous, such as the plates comprising the divertor pump plenums

*Work supported by U.S. Department of Energy under Contract No. DE-AC03-89ER51114.

in DIII–D. Eddy currents are induced where changing poloidal magnetic flux penetrates a conducting component. The flux change is derived from actual disruptions, and is extrapolated linearly with $I_p$ to maximum machine capability. Such components are approximated as thin, flat rectangular plates, for which a standard analytical expression yields the eddy current. The largest loads are produced where the current crosses toroidal magnetic field.

Induced current loads dominate in components that do not receive halo currents.

### 1.2. Halo Current Loads

Halo currents are electric currents flowing in the scrape-off layer (SOL) plasma outside the last closed magnetic surface. Disruptions broaden the SOL, fill it with plasma, induce a large toroidal electric field and drive a large halo current. Halo currents enter and leave the vessel and plasma-facing components (PFC) where they intercept open SOL magnetic lines. Because the halo plasma pressure ($\beta_p$) is low, the halo current is almost force-free and flows nearly parallel to B. Only the poloidal component of the halo current flows into the first wall. Poloidal vessel currents originating in the halo and crossed with the toroidal magnetic field produce larger vessel loads than induced toroidal currents [1] and are the principal drivers of vessel motion during VDE's.

Poloidal halo current to the DIII–D vessel is measured by a set of current monitor resistors interposed between selected graphite armour tiles and the vessel wall [4]. A top view of the present tile current monitor (TCM) array in the bottom of the vessel is illustrated in Fig. 1.

TCM data indicate that the peak halo current $I_{hPk}$ is typically greater during VDEs than other disruptive events. Measurements of the vessel vertical displacement, which is an indicator of global VDE vertical impulse ~ $\int I_P B_T\, dt$, show that the worst case impulse increases linearly with $I_p$ [5]. Continued proportionality to $I_{hPk}B_T$ is assumed to extrapolate to the worst case halo current loads using full $B_T$ and $I_{hPk} = 0.2\, I_p$. This empirical scaling can be justified by a model calculation of the force from the quadrupole shaping field acting on a shrunken, off-center plasma, whose size is set by the observation that VDEs always disrupt at about the same safety factor, $q \sim 2$ [6].

Recent data show that the halo current is nonuniformly distributed toroidally, and the nonuniform structure typically rotates at hundreds of Hz [7]. However, there are occasional examples of nonrotating asymmetries. Fig. 2(a) shows an example of another common behavior, where an initially rotating structure later stops at 1.734 s. The nonuniformity is characterized by a toroidal peaking factor (TPF), TPF = (peak local $J_h$÷ toroidal average $J_h$). The TPF is sometimes very large early in the VDE, when $I_h$ is small. However, the TPFs observed to date are ≤ 3 during the time of greatest interest, when the halo current is large. Fig. 2(b) shows the TPF vs. $I_h(t)$.

These DIII–D halo current data are similar to Alcator C-Mod data [C-Mod]. Toroidal peaking, a recently discovered phenomenon, has been included in DIII–D load calculations.

The halo current is believed to be driven by two fundamental effects: decay of the bulk plasma current which induces toroidal current (and thus produces poloidal current) in the force-free halo region, and reduction in the vacuum toroidal flux linked by the halo region as the plasma cross-section shrinks (which produces a poloidal voltage). Continuing theoretical analysis of the disruption-driven axisymmetric halo current has suggested that

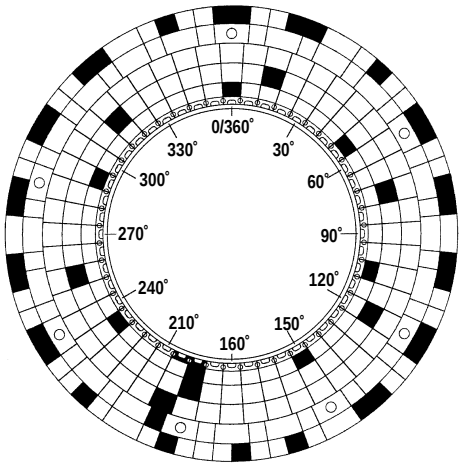


Fig. 1. Array of current monitored tiles in bottom of DIII–D vessel in 1996, viewed from above.

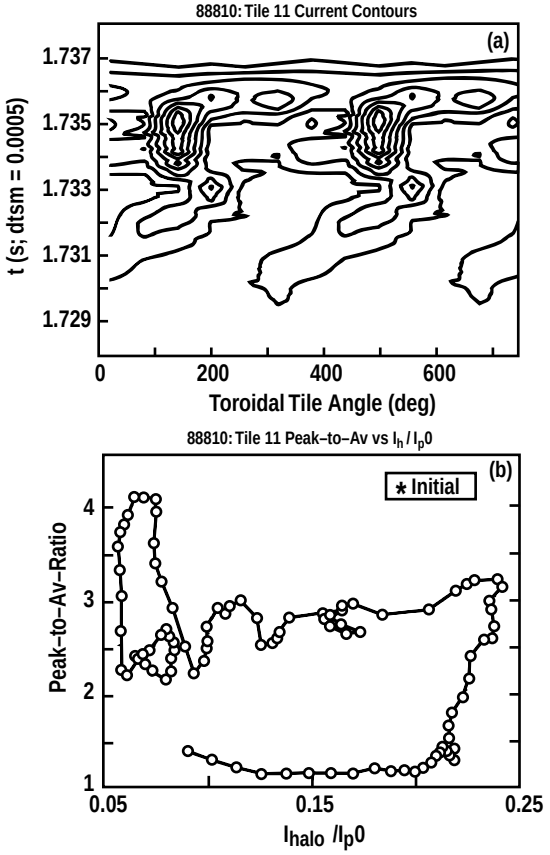


Fig. 2. Toroidal non-uniformity during a VDE. (a) contours of current into tiles versus toroidal angle in second row of tiles from inside vessel. Toroidal angle repeats two periods for viewing ease. Angle from vertical indicates rotation of peak current. (b) evolution of halo current toroidal peaking factor versus halo current normalized to $I_p$. Points are 0.05 ms apart.

the peak axisymmetric component of the halo current is maximized by a high effective growth rate, high bulk plasma current decay rate and initial plasma current, a low edge safety factor during the current quench phase, and a low halo resistance.

## 2. VESSEL LOADS AND DEFLECTIONS

The duration of the peak halo currents is about 2 ms, whereas the time for rise and decay of halo currents is about 15 ms. To evaluate the structural effects of halo current forces, a 3D dynamic analysis of the DIII–D vacuum vessel was completed. To encompass all worst case loading conditions, the magnitude of the halo current was taken as 20 percent of a pre-event 3.00 MA plasma with a 15 ms rise-decay time.

A 2:1 toroidal peaking factor is used on the applied loads in the model. The loads were applied on the floor in one case and on the side of the vessel in the second. The loads vary both radially and circumferentially around the vessel. Also, in the radial direction, the loads decrease linearly with increasing radius. The applied load, $P_{applied}$, is equal to $P_{initial}$ [1 + cosø] with $P_{initial}$ varying from 2.86 bar to 1.03 bar in the radial direction on the floor and varying from 1.03 bar to 0.73 bar on the side of the vessel. The loads are applied as a time pulse and rise from zero to peak halo current in 13 ms and then fall to zero in 2 ms.

The dynamic analysis of the DIII–D vacuum vessel was done to find stresses in the support trunnions, the resultant loads placed on the support trunnion bolts, and vacuum vessel stresses and displacements, due to halo current induced loads in the vessel. The vessel is supported by 4 equally spaced horizontal trunnions extending radially at the vessel midplane.

The 3D finite element model of the vessel was subjected to a halo current of 20% of a 3 MA plasma with a peaking factor of 2. Figure 3 shows a vertical displacement plot at the center of the vessel floor at 0 degrees as a function of time. The maximum vertical displacement is 3.5 mm. The loads on the 4 trunnions were nearly equal.

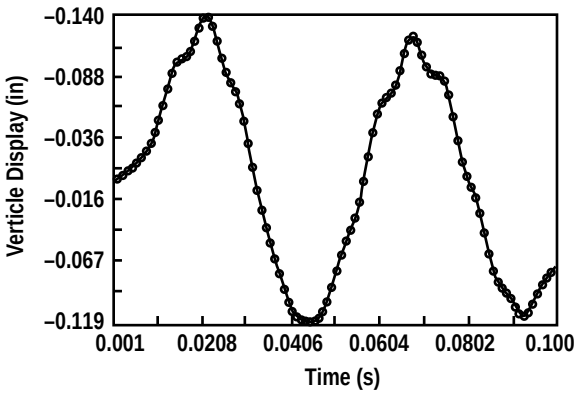


Fig. 3. Model results for halo current induce vessel displacement from a 3 MA plasma.

Measurement of the motions of the vacuum vessel floor have been recorded over the last several years. Plots of the amplitude of the vertical displacements of the vessel versus plasma current are shown in Fig. 4. Since most of the hard disruptions occurred at near maximum toroidal field of 2.2 Tesla, a linear fit through the maximum displacement at each value of plasma current provides the best representation of peak vessel motion.

It is seen that the dynamic analysis results overpredicts the vessel motion. Linear scaling of the measured results indicate a displacement of 0.092 in. vs. the 0.140 in. predicted analytically. This can be partly explained by 2 ms time duration of halo currents with 2:1 peaking factors vs. the 15 ms pulse time used for the dynamic analysis. Based on the conservative structural analysis, it is safe to assume that the DIII–D vacuum vessel can safely react halo current loads resulting from 3 MA plasma operation.

The following procedure is used for the stress analysis of structures in which the design is governed by halo current loads:

1. For preliminary design, apply a static pressure load normal to the plasma facing surface base on 20 percent of a 3 MA plasma, evenly distributed toroidally (no peaking factor). A structural model representing a repetitive sector of the structure is used with a dynamic load factor (DLF) of 1.0 for sizing calculations.
2. Based on the above results, the thickness of the component may be increased or reinforcing ribs and/or gussets added to satisfy the stress allowable for the structure and its supports to the vacuum vessel.
3. Perform a frequency analysis for the reinforced structural model. Using response spectrum curves for impulsively applied loads with a triangular rise-decay time history, determine the DLF for halo currents with a 2:1 peaking factor (2 ms) and symmetric halo current loads (15 ms). Static stress analysis is performed for the sector structural model using the highest pressure loads adjusted for DLF. Various load cases are analyzed for halo current paths that may split on the surface of the component and/or flow through the component supports to the vessel and back to the disrupting plasma.
4. For toroidally continuous structures, the 2:1 peak to average factor for the halo current will produce displacements that are offset globally from the centerline of the vessel. To evaluate these effects, a 180 degrees structural model is required. A frequency analysis is performed to determine the DLF for the 2 ms peaking loads. The equivalent pressure loads, p, are applied statically with p=0 at 0 degrees, p at 90 degrees, and 2p at 180 degrees. A dynamic time-history analysis with a 2 ms impulse load to the structural model is performed if the static analysis does not satisfy the allowable stress values.

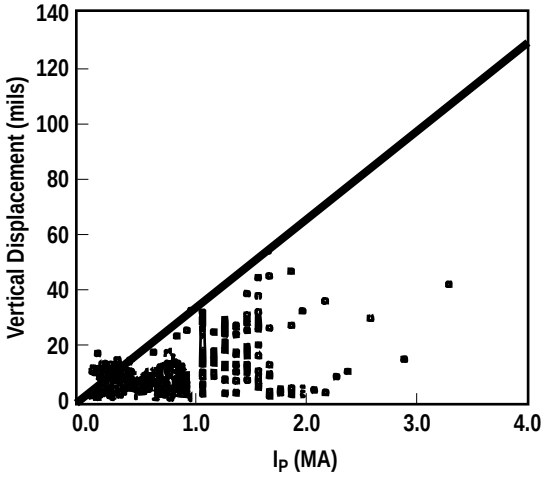


Fig. 4. DIII–D results for vessel vertical deflection versus plasma current.

## REFERENCES


1. E.J. Strait, L.L. Lao, J.L. Luxon, E.E. Reis, Nucl. Fusion **31** (1991) 527.
2. A.G. Kellman *et al.*, in Fusion Technology (Proc. 16th Symposium, London, 1990).
3. M.M. Mennon, M.J. Schaffer, A.G. Kellman, Bull. Am. Physical Soc. **37** (1992) 1570.
4. M.J. Schaffer, B.J. Leikind, Nucl. Fusion **31** (1991) 1750.
5. E.E. Reis *et al.*, in Fusion Engineering (Proc. 12th Symposium, Monterey, CA 1987) vol. **1** IEEE, New York (1987) 212.
6. M.J. Schaffer, unpublished.
7. T.E. Evans *et al.*, to be published in J. Nucl. Materials.
8. R.S. Granetz et al., Nucl. Fusion **36** (1996) 545.